Chain stiffness effect on the properties of topological polymer brushes and the penetration by free chains using MD simulation

Journal of Physics Communications

OPEN ACCESS

RECEIVED
26 September 2017

REVISED
15 December 2017

ACCEPTED FOR PUBLICATION
4 January 2018

PUBLISHED
24 January 2018

PAPER

Chain stiffness effect on the properties of topological polymer brushes and the penetration by free chains using MD simulation

Honghong Lyu[1], **Fuxian Xu**[1], **Holger Merlitz**[1,2] **and Chen-Xu Wu**[1]

[1] Institute of Softmatter and Biometrics, Xiamen University, Xiamen 361005, People's Republic of China
[2] Leibniz Institute of Polymer Research Dresden, D-01069 Dresden, Germany

E-mail: cxwu@xmu.edu.cn

Keywords: polymer brush, chain stiffness, MD simulation

Abstract

Molecular dynamic simulations are carried out to study the static and dynamic properties of topological polymer brushes by taking into account chain stiffness and their topological feature. It is found that chain stiffness plays an important role in topological polymer brushes, and there exists scaling laws for the radius of gyration against chain stiffness and topological feature, indicating that bending interaction is as important as topological constraint. An empirical finitely extensible nonlinear elastic force in terms of chain stiffness and topological features is also obtained by fitting related parameters. A simulation on the invasion of free polymer chains from environment into a ring polymer brush shows that under pressure, such kind of penetration depends largely on chain stiffness, in contrast to the minor influence of topological structure, which seems to be suppressed.

1. Introduction

Recently much attentions have been paid to polymer brushes composed of polymer chains tethered to a substrate surface, which triggered a lot of applications, such as colloidal stabilization, adhesion, biocompatibility, and tribology [1–3]. Since Alexander, de Gennes and Semenov made pioneering investigations on polymer brushes [4–6], a large number of progresses have been made in this field [7]. For topological polymer brushes, using the powerful molecular dynamic simulation (MD) technique, various properties(both static and dynamic) had been studied by taking into account their topological structures and chain stiffness [8, 9]. Theoretically given an example, Sakaue considered many-body effect of topological origin in melt and solution, and obtained an exponent theory by using a mean-field theory [10].

How the chemical nature or primary structure of the main chain influences the brush properties is an important and fundamental question which attracts many researchers' attentions. Typically polymer brushes are classified into two categories: the so-called flexible brushes, in which flexible side chains are grafted onto a flexible main chain, and the rod brushes, in which semiflexible or rodlike side chains are grafted onto the main chain [11]. There are a large number of studies related to the static properties of flexible polymers under the good solvent condition as most synthetic polymers are fully elastic [12–16]. However, recently semi-flexible polymers, especially popular biopolymer such as DNA, rodlike viruses, proteins, or actin filaments, also arouse interest [17–19]. On the other hand, it is found that stiffness also plays an important role when observing synthetic polymers such as polyethylene in the short distance along the chain. Similar influences can also be found in the system of a polymer brush covered by a layer of linear polymer chains under pressure.

Marine biofouling, defined as the accumulation of marine micro- and macro-organisms on man-made surfaces, still drive scientists' heart, as it affects maritime and aquatic industries [20]. A variety of functional polymer brushes and coatings have been developed for combating marine biofouling and biocorrosion with much less environmental impact than traditional biocides. In order to study how substances such as marine algae entering a coating surface, we analyze dynamic properties of polymer brushes composed of polymer chains with different stiffness, topological structures after covered by a layer of linear polymer chains under pressure. There exists similar model about the healing of polymer interfaces, as reported by Ge *et al* [21], where they varied

the entanglement length by the chain stiffness, but their two separate films are cut by one polymer sample, which is different from our simulation condition.

In our previous study, we investigated how topological feature influences end-monomer distribution by constructing topological polymer chains, with the number of rings featuring the topological constraint of chain [22]. In this paper, using MD simulation, we study how chain stiffness affects the properties of polymer brushes with different topological constraints. In a facilitated way, a persistence length l_p is used to characterize the contribution of bending energy (chain stiffness). In addition, in order to simulate the invasion of exteriors from environment to the brush, we also investigate the dynamic properties of polymer brush by covering a layer of free chains atop and carrying out a vertical compression. In section 2, the polymer brush model is explained and relevant parameters are set. The static properties of polymer brush are discussed in sections 3.1 and 3.2 presents the chain energy and bond force in the system. Section 3.3 analyzes the penetration behaviors for a polymer brush covered by linear chains atop. A summary is presented in section 4.

2. Simulation model and tool

The polymer brushes we study consist of an array of 10×10 polymer chains (122 monomers per chain) with one end grafted onto a substrate. Such an array size we chose is large enough statistically, as shown in our previous report [22]. Computer simulations were performed using the open source molecular dynamics package LAMMPS, and a periodic boundary condition was chosen to impose along both x and y directions on the box $50 \times 50 \times 200$ we set. The brushes were artificially constructed based on the coarse-grained bead-spring model, with all beads governed by potentials U_{LJ}, U_{FENE}, U_{WALL} and U_{BEND} respectively, i.e.

$$U_{tot} = U_{LJ} + U_{FENE} + U_{WALL} + U_{BEND}, \tag{1}$$

where the first term stands for the shifted Lennard-Jones (LJ) interaction between two non-bond monomers, the second term reflects the finite extensible nonlinear elastic potential for neighboring bonds, the third term exhibits the repulsive interaction between polymer chains and substrate (WALL), and the last one comes from the bending effect.

The shifted LJ potential given by

$$U_{LJ}(r) = 4\epsilon\left[\left(\frac{d}{r}\right)^{12} - \left(\frac{d}{r}\right)^{6} - \left(\frac{d}{r_c}\right)^{12} + \left(\frac{d}{r_c}\right)^{6}\right], \tag{2}$$

takes into account only a short-range repulsive potential via a cut-off, an operation widely used to simulate polymer brushes in a good solvent. Here $\epsilon = 1.0$, $d = 1.0$, $r_c = 1.124$ is the depth of potential, d is the bead diameter, r is the distance between particles, and r_c denotes the cutoff distance. Evidently, solvent quality is one of important contributors to the conformations and behaviors of polymer brushes. In a good solvent, for example, where a repulsive interaction between polymer monomers and solvent molecules is favorable, the entropy loss due to overlapping of chains will cause polymer chains to expand as much as they can.

Besides the non-contact interaction, neighboring beads along the polymer chains are connected through a finitely extensible nonlinear elastic (FENE) bond potential [23]

$$U_{FENE} = -0.5KR_0^2 \ln\left[1 - \left(\frac{r}{R_0}\right)^2\right] + 4\epsilon\left[\left(\frac{\sigma}{r}\right)^{12} - \left(\frac{\sigma}{r}\right)^{6}\right] + \epsilon, \tag{3}$$

where the coefficient $KR_0{}^2$ represents the energy scale of interaction (typical values $K = 30$ and $R_0 = 1.5$), with R_0 the maximum bond length, r is the variable bond length, and the 2nd repulsive term is cutoff at $2^{1/6}\sigma$, the minimum of the LJ potential ($\epsilon = 1.0$ and $\sigma = 1.0$). The FENE multibead-spring model is a successful coarse-grained approach that captures the basic physical behaviors of polymeric systems [24, 25]. In our simulation model, bond length is set as $l_v = 0.97$ on average.

To demonstrate the strong repulsion by the substrate, the first monomer (grafted monomer) grafted at a substrate located at $z = 0$ is modeled by a 9-3 type LJ-wall potential

$$U_{WALL} = \epsilon\left[\frac{2}{15}\left(\frac{d}{r}\right)^{9} - \left(\frac{d}{r}\right)^{3}\right](r < r_c), \tag{4}$$

with $\epsilon = 1.0$ and $r_c = 0.858$.

As usual, a harmonic-style potential

$$U_{\mathrm{BEND}} = \eta(\theta - \theta_0)^2 \tag{5}$$

is used to represent the bending energy, a contributor correlated with persistence length describing chain stiffness. Here $\theta_0 = 150$ is the equilibrium value of bending angle between neighboring bonds, and η is a pre-factor, in which usually a factor of $1/2$ is included. From the cosine of the angle formed between neighboring bonds

$$\langle \cos\theta \rangle = \frac{\int_{\theta_0}^{2\pi} \cos\theta \mathrm{e}^{-\eta(\theta-\theta_0)^2} \sin\theta \mathrm{d}\theta}{\int_{\theta_0}^{2\pi} \mathrm{e}^{-\eta(\theta-\theta_0)^2} \sin\theta \mathrm{d}\theta}, \tag{6}$$

and the correlation

$$l_{\mathrm{p}} = \frac{l_0}{1 - \langle \cos\theta \rangle}, \tag{7}$$

we obtain

$$l_{\mathrm{p}} = \frac{l_0}{1 - f(\eta)}. \tag{8}$$

As the bending stiffness η can be determined once l_{p} is specified, in this paper we use persistence length l_{p} to discuss chain stiffness.

To study the contribution of bending energy in such a polymer brush system, for simplicity, we use persistence length as the primary variables instead of equation (5). In addition, to feature the topological structure of the polymer brush, we define a topological constraint using ring number rn(=1, 2, 3, 4, 5, 6), as reported in our previous study [22]. The total number of monomers in each polymer chain is kept unchanged while we investigate the ring number dependence. In our system, the motion for any effective monomers (non-grafted monomer) is governed by Langevin equation

$$m\frac{\mathrm{d}^2\mathbf{r}_i}{\mathrm{d}t^2} + \varsigma\frac{\mathrm{d}\mathbf{r}_i}{\mathrm{d}t} = -\frac{\partial U_{\mathrm{TOT}}}{\partial \mathbf{r}_i} + \mathbf{F}_i, \tag{9}$$

where $m = 1$ is the monomer mass, r_i is the position of the ith monomer, ς is the friction coefficient, and $\mathbf{F}_i$ is a random Gaussian force adapting the system for the heat bath, and obeying the correlation function $\langle \mathbf{F}_i(t) \cdot \mathbf{F}_j(t') \rangle = 2k_{\mathrm{B}}T\varsigma\delta_{ij}\delta_{\alpha\beta}$. In our simulation, the diameter of monomers is $d = 1.0$, and $K_{\mathrm{B}}T = 1.2\epsilon$, where k_{B} is Boltzmann constant and T is the absolute temperature. Each time step was set to be $\Delta t = 0.0015\tau_{\mathrm{LJ}}$, with $\tau_{\mathrm{LJ}} = (md^2/\epsilon)^{1/2}$ being the LJ time, and a friction coefficient $\varsigma = {\tau_{\mathrm{LJ}}}^{-1}$ was implemented. The brush conformation was initialized as an array of stretched chains before the system reachs an equilibrium state by implementing 2×10^8 simulation steps.

To simulate the biofouling due to invasion of exteriors coming from its environment under pressure, we also use a 10×10 ring polymer brush with a grafting density of 0.075 (0.15 for corresponding linear brush) with each ring composed of 122 monomers. Then 2400 free linear chains (10 monomers each) are used to simulate a layer formed due to the external environment, which is covered by a wall atop moving slowly downward until the density of free chains reaches 0.3, a value corresponding to dense but semidilute state. Here it should be noted that this is just for simplicity and in many cases the fouling material actually consist of proteins that represented by stiff polymer-molecules [26]. The density distributions are calculated after linear polymers invade the brush and the system reaches its equilibrium, and a comparison of density distribution between ring polymer brush and linear polymer brush is made.

3. MD simulation results and discussion

3.1. Static properties

Since the topological effect in monomer density profile has been studied previously [22], we begin our discussion on the profiles of polymer brushes at different persistence length, as shown in figure 1. It is found that all these curves meet at one fixed point except when the persistence length is zero, and more specifically, there are more monomers in the lower region (lower than the intersection). However, this phenomenon seems to fade away in the long persistence length regime, where the conformations of brush chains become loose due to the decrease of bond support, leading to a decondensation (relatively average distribution) of monomers close to the substrate. Besides, the typical features of monomer density shown here agree with Milchev and Binder's observation [27], including an oscillation of monomer density nearly $z = 0$ due to a 'layering effect' (like the packing of hard spherical particles at a repulsive wall) mentioned in many related simulations [28].

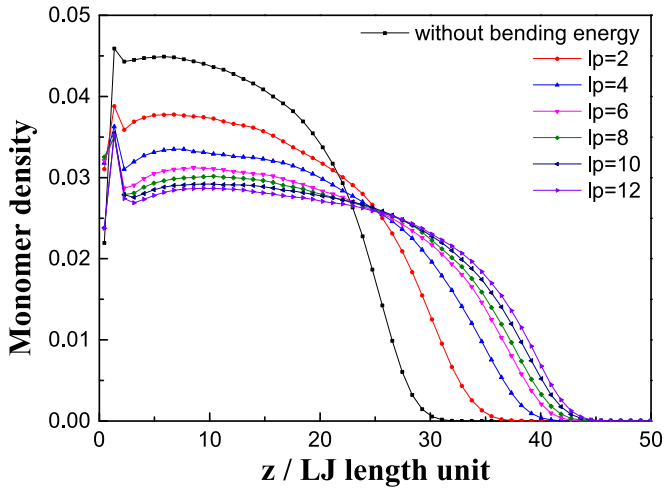

Figure 1. Monomer density profiles along the z-direction for one-ring polymer chains with different persistence lengths.

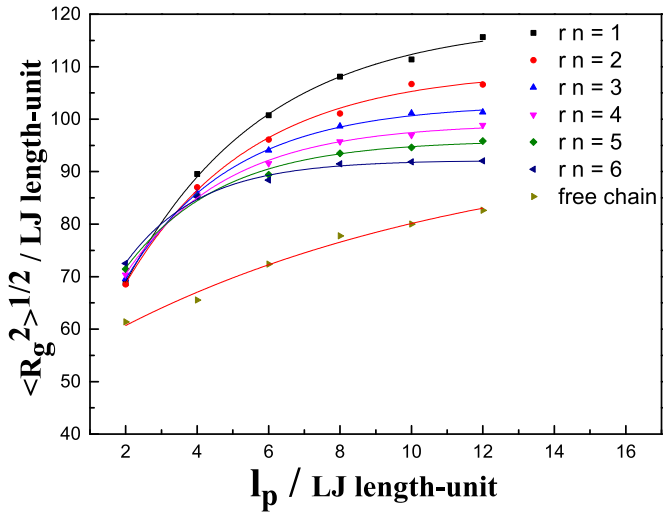

Figure 2. The radius of gyration $\langle R_G^2\rangle^{1/2}$ for polymer brushes at different ring numbers when the persistence changes (chain length $N = 122$) and a free polymer chain also plotted as a comparison.

In order to gain more insight into such polymer chains, we also plot their mean square radius of gyration $\langle R_G^2\rangle^{1/2}$, which is defined as

$$\langle R_G^2\rangle^{1/2} = \left(\frac{1}{N}\sum_{i=1}^{N}\langle(r_i - r_{cm})^2\rangle\right)^{1/2} = \left(\frac{1}{N^2}\sum_{j=1}^{N}\sum_{i=1}^{N}\langle(r_i - r_j)^2\rangle\right)^{1/2}, \quad (10)$$

against persistence of length, as shown in figure 2. Here r_{cm} and r_i represent the center-of-mass position of the polymer chain and radius vector of monomer position in z axis respectively. From the figure it is found that when persistence length increases, the radius of gyration reflecting the size of chains also increases as a result of the excluded volume effect, which dominates other interactions when the radius of gyration reaches the saturated value. Looking at the curves in the figure, it is easy to guess an empirical law

$$\langle R_G^2\rangle^{1/2} = A_1 - A_2 \cdot e^{-kl_p}, \quad (11)$$

fitting the gyration of ring polymer chain against persistence length. The physics hidden behind this still needs to be investigted. Here A_1, A_2, and rn are parameters related to ring number, as presented in table 1. From figure 3, it is interesting to find that A_1, A_2, and l_p all reveal a linear dependence against topological constraint rn.

Table 1. Parameters as a function of ring number.

rn	A_1	A_2	k
1	123.55	76.07	0.19
2	113.14	63.92	0.21
3	105.58	54.95	0.25
4	101.02	49.29	0.27
5	97.50	42.97	0.28
6	93.34	37.92	0.34

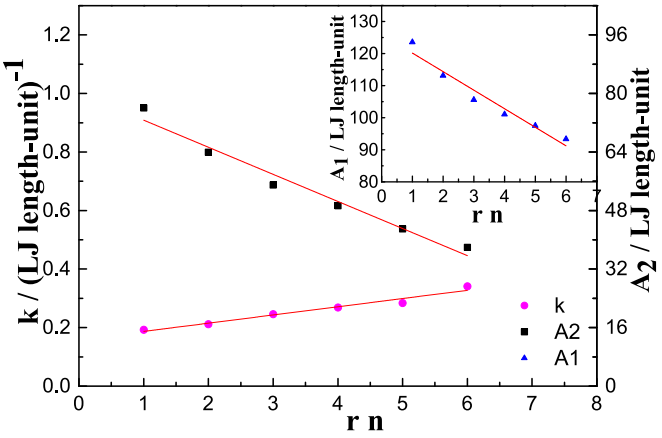

Figure 3. The topological dependence of fitting parameters A_1, A_2, and k (chain length $N = 122$).

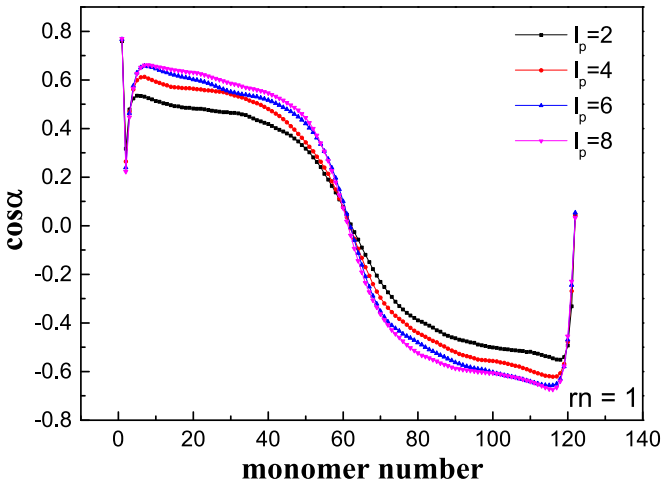

Figure 4. cos α varies against monomer number for different persistence lengths.

$$\langle R_G^2 \rangle^{1/2} = (125.94 - 5.79 \times \mathrm{rn}) - (80.11 - 7.41 \times \mathrm{rn}) \cdot \mathrm{e}^{-(0.16+0.028\times \mathrm{rn})l_p}. \quad (12)$$

It is necessary to note that the fitting parameters are mathematically a complicated function of topological constraint, but consequently the linear part (of Taylor expansion) plays a dominant role, indicating an interesting and simple relation.

In order to demonstrate the conformation of single-ring chain, we also calculated the averaged angle made between bonds and z axis against monomer number, as shown in figure 4. One can imagine that if the one-ring chain forms into an exact circle, cos α will become a standard cosine curve against monomer number in the ring. Specifically, when adding more stiffness into the polymer brushes, the cos α curve will be more close to standard cosine curve as a result of the bond support.

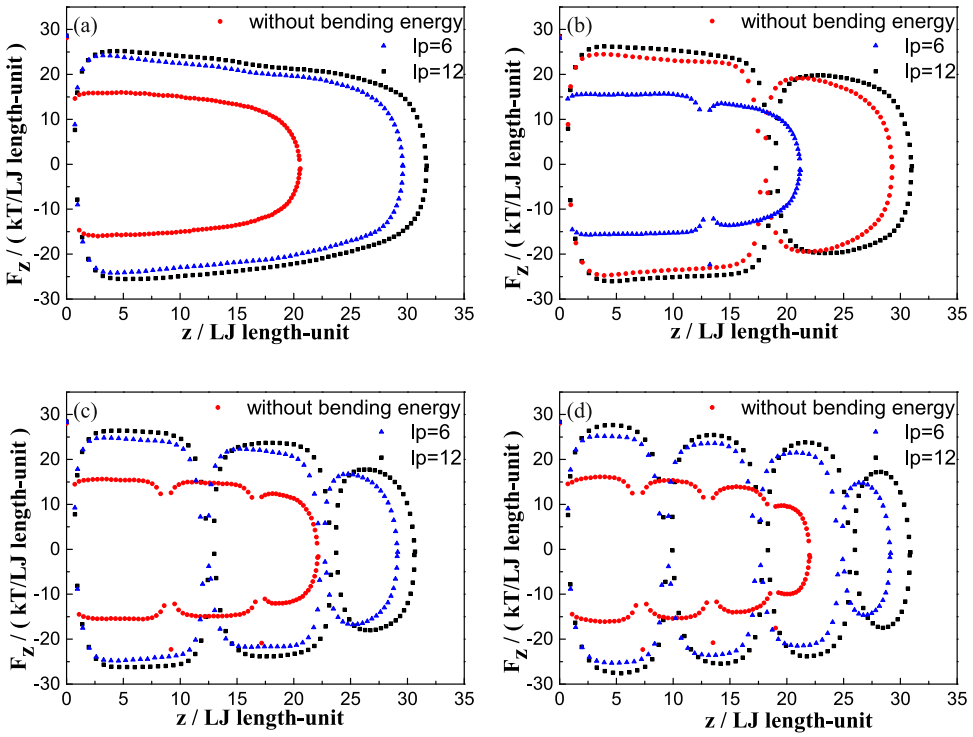

Figure 5. Averaged bond forces along the z direction for ring polymer brush (chain length $N = 122$) at different persistence lengths for various topological constraint values rn as a function of the distance from the surface. (a) Single-ring polymer brushes. (b) Two-ring polymer brushes. (c) Three-ring polymer brushes. (d) Four-ring polymer brushes.

3.2. Chain energy and bond force

After the static features of topological polymer brushes are discussed, it is worthwhile to study the dynamic properties, such as force and energy so as to obtain a complete picture of such systems. Once the interaction potentials are given, it is easy to calculate the force for each monomer:

$$F = -\langle \nabla U_{\mathrm{FENE}}(\mathbf{r}) \rangle = \left\langle -\mathbf{r}\left(\frac{KR_0^2}{r^2 - R_0^2} + \frac{4\varepsilon}{r^2}\left[12\left(\frac{d}{r}\right)^{12} - 6\left(\frac{d}{r}\right)^{6} \right] \right) \right\rangle. \tag{13}$$

Figure 5 exhibits the z-component force that each monomer subjects to as a function of chain stiffness. It is clear that when polymer chains are more flexible, corresponding to a smaller persistence length, and hence leading to a smaller contribution of bond force due to bending energy. In addition, it is also found that the bond force of monomers close to the substrate is larger than that far from it, due to the large volume-excluded effect. And the reason why the force can be positive and negative at the same distance from the surface is that monomers are symmetric about the mid-monomer (branching point) of the ring and experience opposite force.

It is also easy to obtain the FENE stretching energy once the bond force is integrated over z direction, as shown in figure 6 for various topological polymer brush at different persistence lengths. In order to find the exponential power law for FENE stretching energy, we also create a trial function as usual

$$U_{\mathrm{FENE}} = A_1 - A_2 \cdot \mathrm{e}^{-kl_{\mathrm{p}}}, \tag{14}$$

where parameters A_1, A_2, and k are all ring number-dependent, and calculable, as shown in table 2.

From table 2, it is easy to plot figure 7, where parameters A_1, A_2, and l_{p} are found to, as previously noticed, linearly depend on ring number. Thus an empirical function

$$U_{\mathrm{FENE}} = (12.62 - 0.59 \times \mathrm{rn}) - (8.10 - 0.68 \times \mathrm{rn}) \cdot \mathrm{e}^{-(0.15+0.018\times \mathrm{rn})l_{\mathrm{p}}} \tag{15}$$

can be obtained. More detailed insights into such dependence still needs to be gained.

3.3. Isothermal compression of polymer brush

In order to study the invasion from environment to polymer brush under pressure, like marine biofouling, we cover a ring polymer brush with a layer of free linear chains under an external pressure, which makes the

Table 2. Fitting parameters for FENE force as a function of ring number.

rn	A_1	A_2	k
1	11.95	7.41	0.18
2	11.40	6.72	0.19
3	10.88	5.99	0.19
4	10.40	5.51	0.20
5	9.79	4.75	0.21
6	8.86	3.94	0.29

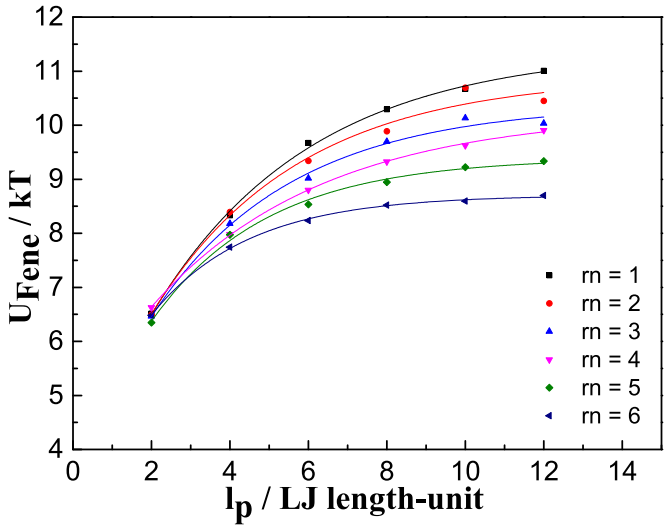

Figure 6. Stretching energy scaled with chain length as a function of persistence length and topological constraint.

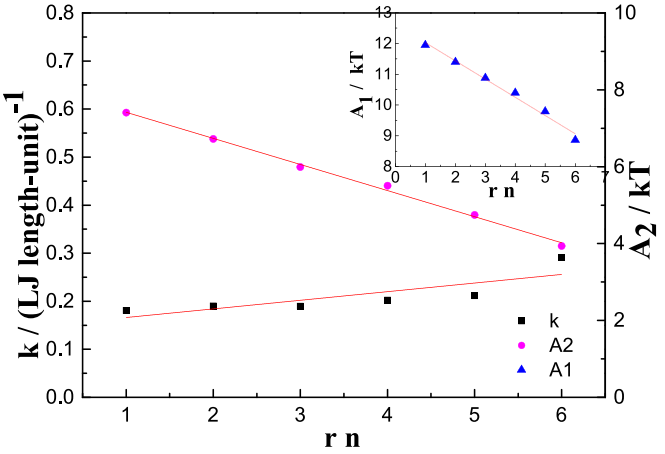

Figure 7. The fitting parameters of A_1, A_2, and k for FENE force linearly depends on topological constraint (chain length $N = 122$).

monomer density (nearly 0.30) far greater than previous situation (nearly 0.03), corresponding to a dense but semidilute brush. By slowly compressing the wall at the top of free chains, we study the invasion of linear chains into one-ring polymer brush via computer simulation. It is observable from figure 8 that when polymer chains in the brush become stiffer, linear free chains are more likely to penetrate polymer brush semidilute solution, judged by the enlarged overlapping area between brush chains and free chains. Here, the main reason is probably the lower monomer density of the brush at $l_p = 10$. A second contribution may be the penalty on conformational entropy: while flexible chains are losing quite a bit conformational entropy when entering a brush (because they

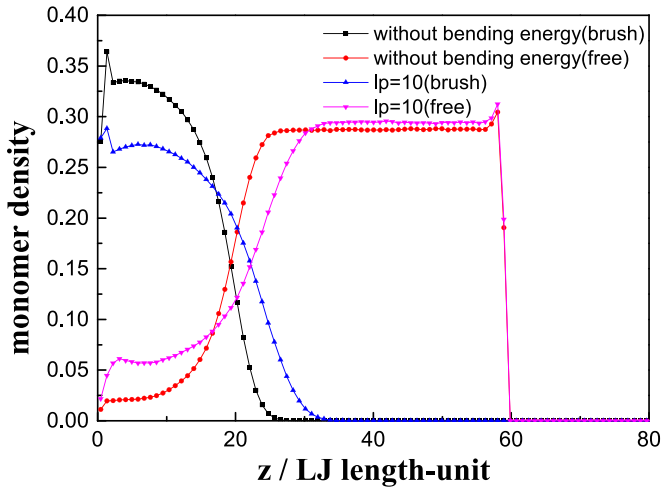

Figure 8. Profile of grafted monomers and free monomers with persistence lengths of 0 and 10 for one-ring polymer brush.

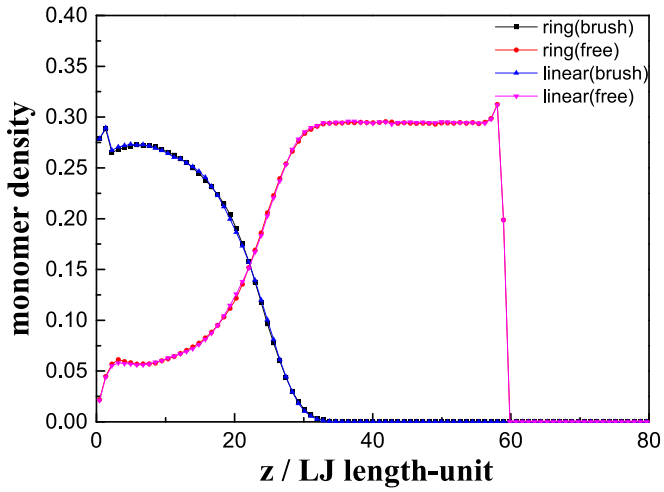

Figure 9. Profile of grafted monomers and free monomers with persistence length of 10 for linear or one-ring polymer brush.

are preferably oriented in vertical direction and thus losing flexibility), chains with $l_p = 10$ have little to lose in that respect and may enter the brush without much entropic penalty.

On the other hand, it is also interesting to investigate the topological dependence of such invasion system under pressure, given a fixed persistence length. In the simulation, we open the ring-type polymer brushes so as to form a linear polymer brush, then plot the monomer profile, as shown in figure 9. It is found that there is no significant difference before and after the operation, in contrast with the apparent dependence on stiffness, indicating that there are no significant differences in the contributions of conformational entropy to both setups. When the ring number changes, similar results are found (with no significant difference between ring and free chains in figure 10), indicating that topological constraints do not significantly alter either the conformational entropy changes (of molecules in and outside the brushes) in the two setups and pressure suppresses the brush topological dependence during the invasion process of free chains from environment to polymer brushes. Here it is worthwhile to mentioned that in many cases fouling materials consist of proteins that are represented by stiff polymer molecules [26], which affects the inclusion energy and thus the penetration of molecules in the brush [29].

4. Conclusions

Using LAMMPS for simulation, we study the chain stiffness effect on the static and dynamic properties of topological ring polymer brushes under different topological constraints. Empirical expressions for various static and dynamic properties, including scaling laws, for such polymer brushes are obtained in terms of chain

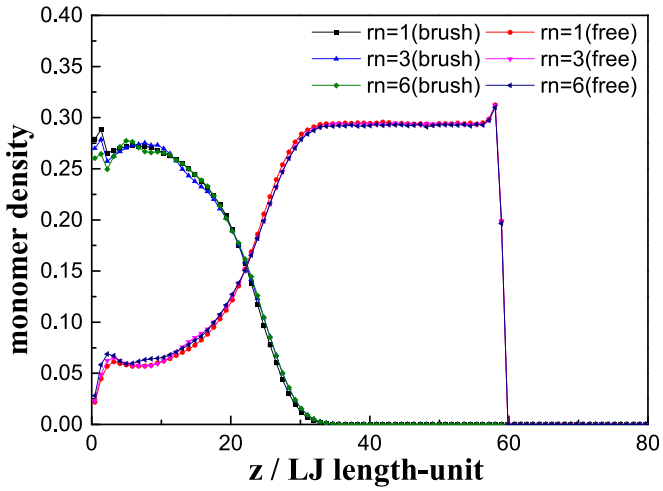

Figure 10. Profile of grafted monomers and free monomers with persistence length of 10 for polymer brush with ring numbers 1, 3, 6 respectively.

stiffness and topological constraint. An isothermal compression simulation shows that chain stiffness plays an important part during the penetration process of free chains from environment to topological ring polymer brushes, while the dependance of polymer brushes on their topological features seems to be suppressed by pressure during such an invasion process.

ORCID iDs

Chen-Xu Wu https://orcid.org/0000-0002-3984-3297

References

[1] Napper D H 1986 *Polymeric Stabilization of Colloidal Dispersions* (New York: Academic) (https://doi.org/10.1002/pi.4980180420)
[2] Hucknall A, Simnick A J, Hill R T, Chilkoti A, Garcia A, Johannes M S, Clark R L, Zauscher S and Ratner B D 2009 Versatile synthesis and micropatterning of nonfouling polymer brushes on the wafer scale *Biointerphases* **4** FA50–7
[3] Auroy P, Auvray L and Léger L 1991 Characterization of the brush regime for grafted polymer layers at the solid–liquid interface *Phys. Rev. Lett.* **66** 719
[4] Alexander S 1977 Adsorption of chain molecules with a polar head *J. Phys.* **38** 983–7
[5] de Gennes P G 1980 Conformations of polymers attached to an interface *Macromolecules* **13** 1069–75
[6] Semenov A N, Vlassopoulos D, Fytas G, Vlachos G, Fleischer G and Roovers J 1998 Dynamic structure of interacting spherical polymer brushes *Langmuir* **15** 358–68
[7] Lee H S and Penn L S 2016 *In situ* study of polymer brushes as selective barriers to diffusion *Macromolecules* **41** 8124–9
[8] Lee S and Spencer N D 2007 Achieving ultra-low friction by aqueous, brush-assisted lubrication *Superlubricity* (Zurich: Elsevier) (https://doi.org/10.1016/B978-044452772-1/50052-4)
[9] Li A 2013 Structure-property relationships of surface-grafted polymeric architectures *PhD Thesis* ETH Zurich https://doi.org/10.3929/ethz-a-009794990
[10] Sakaue T 2011 Ring polymers in melts and solutions: scaling and crossover *Phys. Rev. Lett.* **106** 167802
[11] Kikuchi M, Le T N L, Narumi A, Jinbo Y, Izumi Y, Nagai K and Kawaguchi S 2008 Conformational properties of cylindrical rod brushes consisting of a polystyrene main chain and poly(n-hexyl isocyanate) side chains *Macromolecules* **41** 6564–72
[12] Grosberg A Y, Khokhlov A R, Stanley H E, Mallinckrodt A J and Mckay S 1995 Statistical physics of macromolecules *Phys. Today* **48** 92–3
[13] Jannink G and Cloizeaux J D 1990 Polymers in solution *J. Phys.: Condens. Matter* **2** 1–24
[14] Bower D I and Solis F J 2002 Chapter 6 *An introduction to polymer physics* 71 (Cambridge: Cambridge University Press) 9780521637213
[15] De Gennes P G and Witten T A 1980 Scaling Concepts in Polymer Physics Scaling Concepts in Polymer Physics **33** 51–54
[16] Schäfer L 1999 *Excluded Volume Effects in Polymer Solutions* (Berlin: Springer) (https://doi.org/10.1021/ma981915p)
[17] Bustamante C, Marko J F, Siggia E D and Smith S 1994 Entropic elasticity of phage dna *Science* **265** 1599–600
[18] Ks J, Strey H, Tang J X, Finger D, Ezzell R, Sackmann E and Janmey P A 1996 F-actin, a model polymer for semiflexible chains in dilute, semidilute, and liquid crystalline solutions *Biophys. J.* **70** 609–25
[19] Ober C K 2000 Shape persistence of synthetic polymers *Science* **288** 448–9
[20] Yang W J, Neoh K G, Kang E T, Teo L M and Rittschof D 2014 Polymer brush coatings for combating marine biofouling *Prog. Polym. Sci.* **39** 1017–42
[21] Ge T, Robbins M O, Perahia D and Grest G S 2014 Healing of polymer interfaces: interfacial dynamics, entanglements, and strength *Phys. Rev.* E **90** 012602
[22] Wan W B and Wu C X 2016 Static and dynamic properties of polymer brush with topological ring structures: molecular dynamic simulation *Chin. Phys.* B **25** 106101
[23] Kremer K and Grest G S 1990 Dynamics of entangled linear polymer melts: a molecular dynamics simulation *J. Chem. Phys.* **92** 5057–86

[24] Grest G S 1996 Interfacial sliding of polymer brushes: a molecular dynamics simulation *Phys. Rev. Lett.* **76** 4979–82
[25] Kroger M 2004 Simple models for complex nonequilibrium fluids *Phys. Rep.* **390** 453–551
[26] Callow M E and Callow J E 2002 Marine biofouling: a sticky problem *Biologist* **49** 10–4
[27] Milchev A and Binder K 2012 Semiflexible polymers grafted to a solid planar substrate: changing the structure from polymer brush to 'polymer bristle' *J. Chem. Phys.* **136** 905
[28] Deb D, Winkler A, Yamani M H, Oettel M, Virnau P and Binder K 2011 Hard sphere fluids at a soft repulsive wall: a comparative study using monte carlo and density functional methods *J. Chem. Phys.* **134** 67
[29] Beer S D, Mensink L I S and Kieviet B D 2016 Geometry-dependent insertion forces on particles in swollen polymer brushes *Macromolecules* **49** 1070